SAND2014-0869P

Atomic Physics for Broadband, Small Active Volume Atomic Magnetometer

Yuan-Yu Jau

Sandia National Laboratories

February 05, 2014

Advantages of Atomic Magnetometer

- Before the high sensitivity atomic magnetometer (AM) was developed, the best magnetic field sensor is superconductor quantum interference device (SQUID), which is able to detect magnetic field at a few fT (10^{-15} tesla)/√Hz with MHz detection bandwidth using very small active volume.
- Since early 2000's, AMs with fT/√Hz and sub-fT/√Hz sensitivities have been demonstrated with detection bandwidth ranging from 1 to 100s Hz. The active volume is from a few mm^3 to a few cm^3.
- Comparing to SQUID, the major advantages of AMs are no requirement of liquid He coolant, sub-fT/√Hz detection, and short-distance sensing.
- AM is therefore very useful in 1.Biomagnetic detections (magnetocariography, magnetoencephalography, and other nerve and muscle activities); 2. Tracking of magnetic nanoparticles; 3. Analysis of magnetic property and structure.

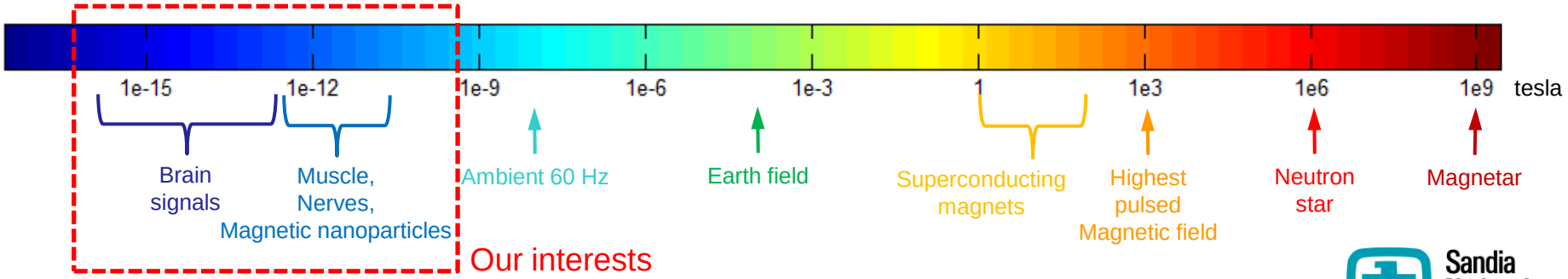

Sandia National Laboratories

Sandia Atomic Magnetometer Project

- Construct a magnetoencephalography (MEG) system using AM technology
- Achieve sensitivity level ≤ 10 fT/√Hz and detection bandwidth ≥ 100 Hz from a small active volume
- Fiber, electrical wires coupled sensors
- 2D Transverse field sensing, gradiometry capability

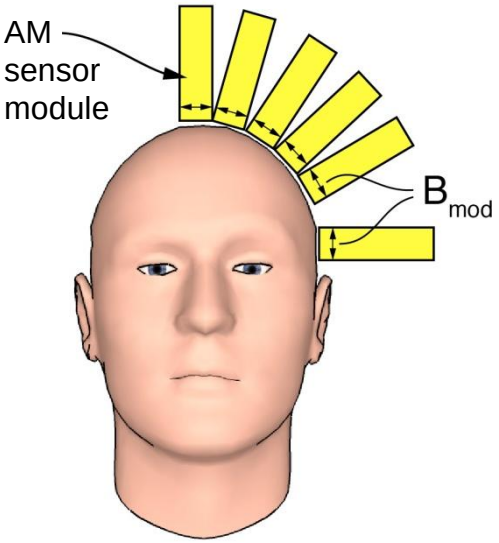

4-Channel Sensor Module

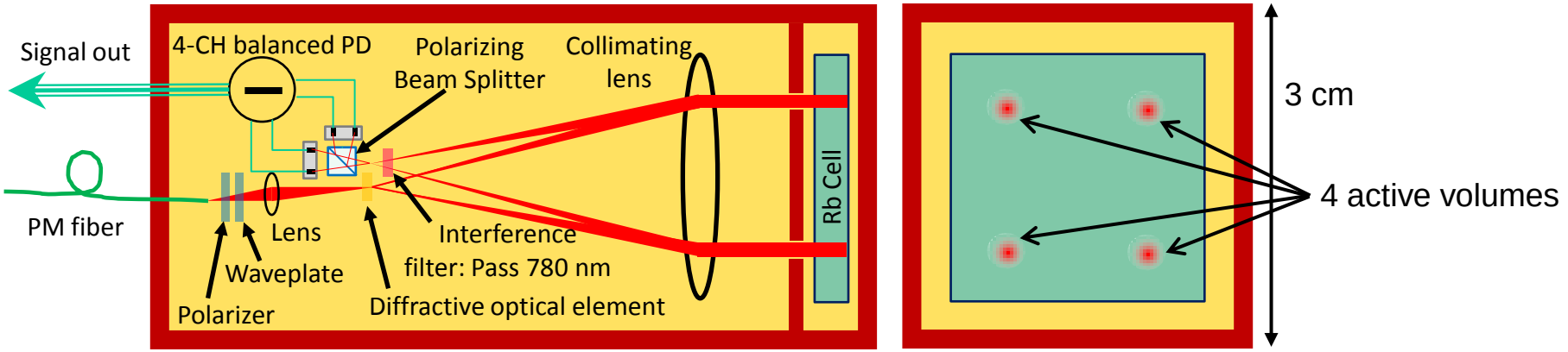

Long-side view

Sensing side
bottom view

Sandia National Laboratories

Human Scale AM MEG System

- 36-channel AM array, reconfigurable (position, head size)
- Human-sized shield, cheaper/smaller installation
- Compare AM and SQUID recordings of human subjects
- Collaboration with MRN, UNM hospital, Candoo Systems

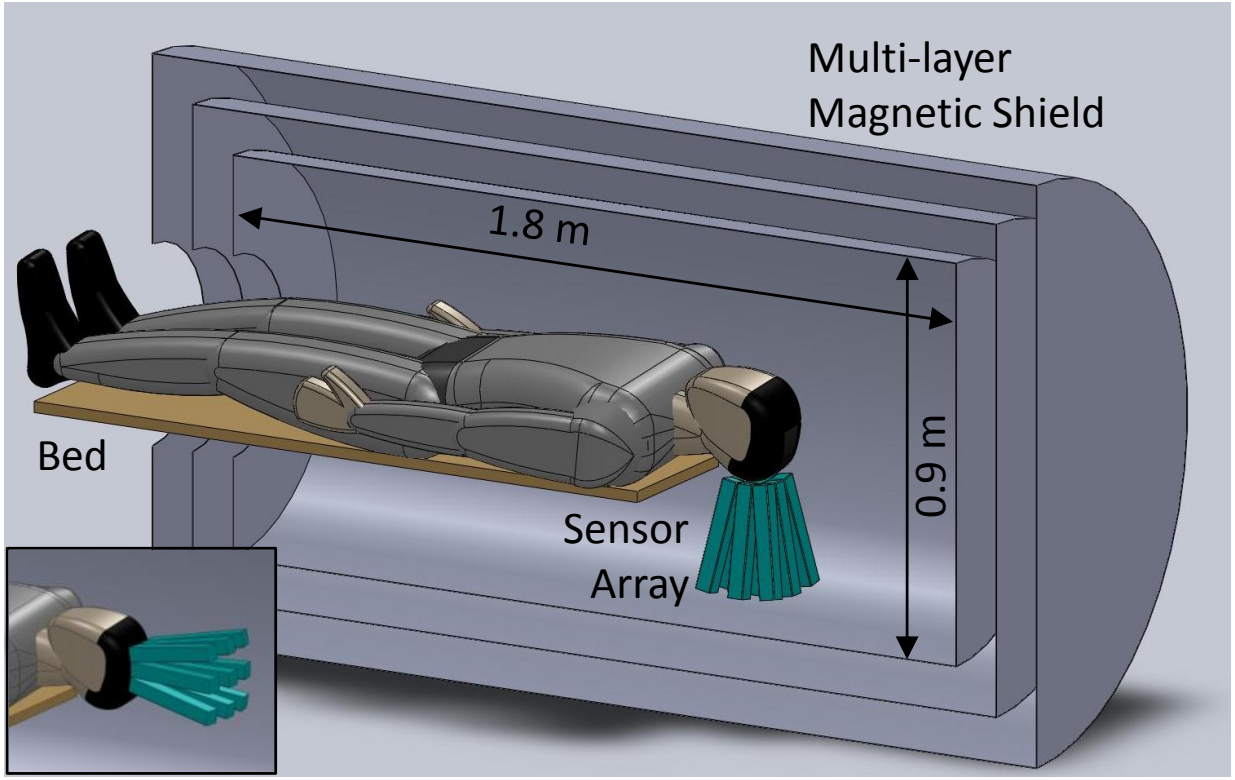

Sandia National Laboratories

Mapping Cortex Activity with Magnetometer Array

- Brain activity on the cortex can generate current dipoles
- The corresponding magnetic-field pattern is picked up by the sensor array
- Different algorithms for inverse problem combining with dipole fittings can be used to localize the sources of the current dipoles

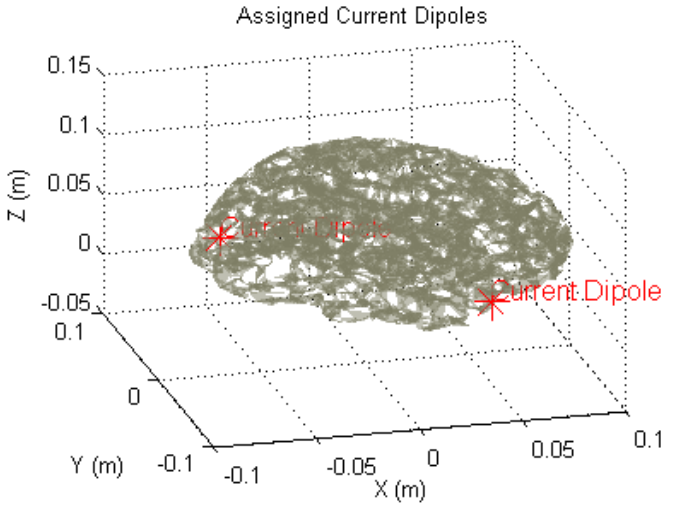

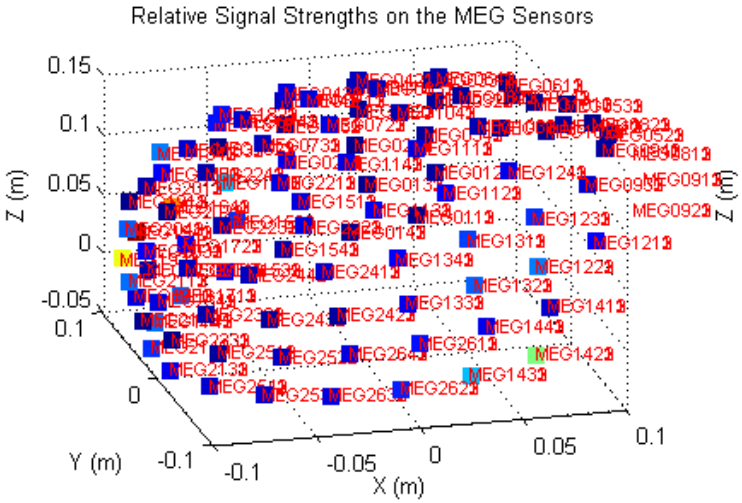

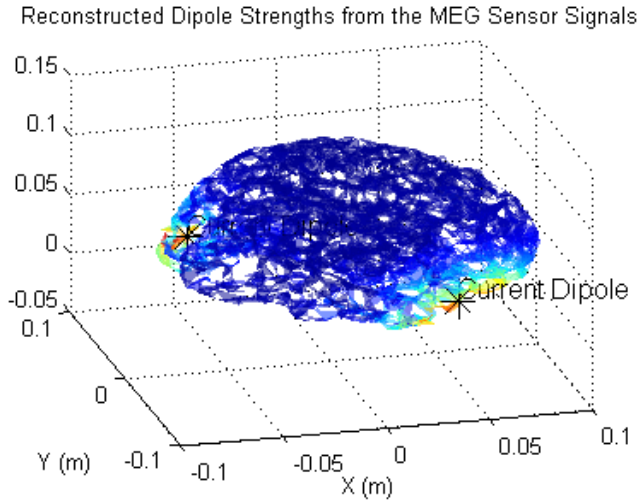

Sandia National Laboratories

Magnetic Nano-Particle Localizations

Magnetic nano-particles

24.75 ±- 0.80 nm

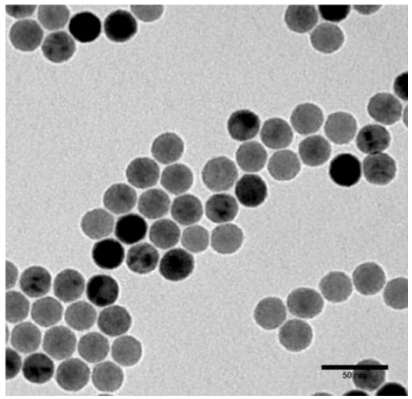

Label with biomarker

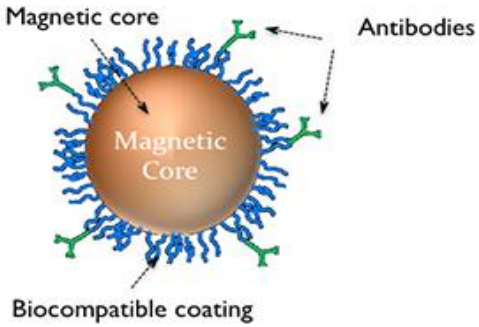

Simulation of nano-particle localizations using AM sensor array

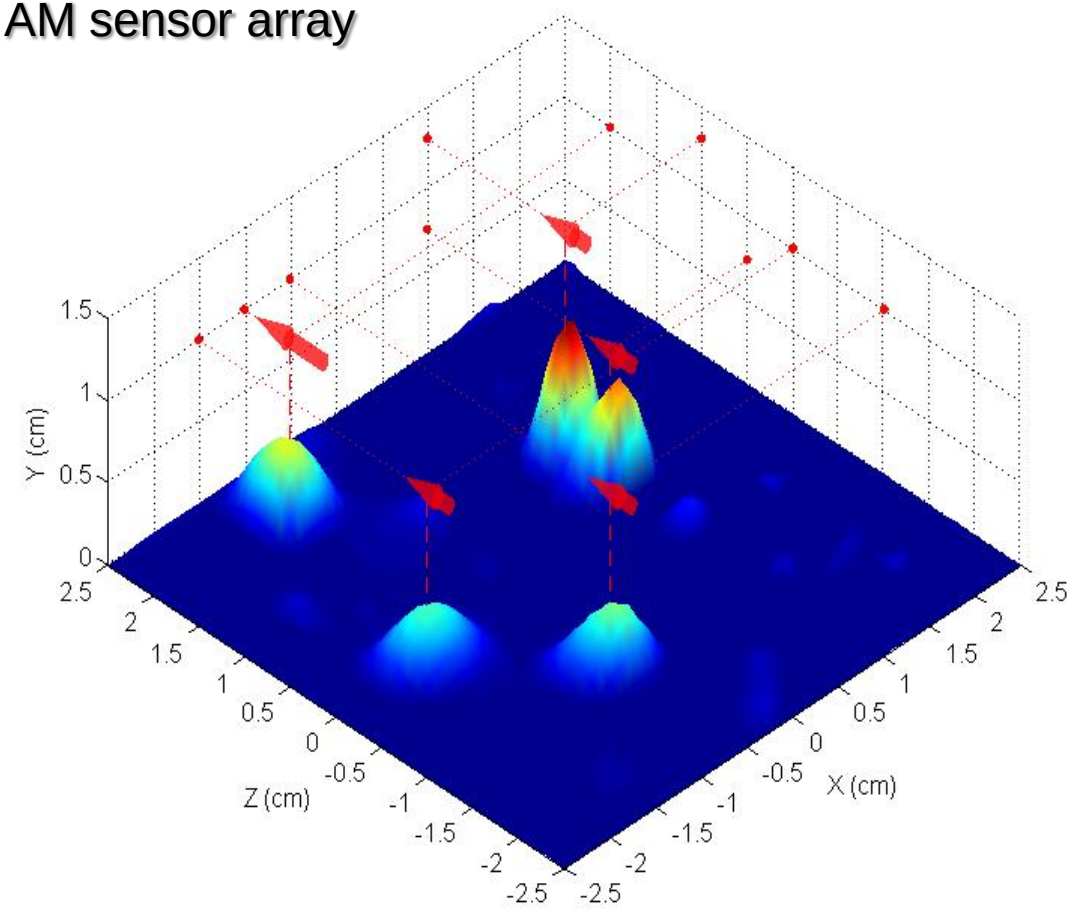

Sandia National Laboratories

Fundamental Sensitivity of AM

Fundamental sensitivity of atomic magnetometer by probing a magnetic resonance from classical atomic spins is limited by the measurement uncertainty:

$$\delta B \sim \frac{1}{\gamma\sqrt{nVT_2\tau}}$$

Here, γ is the gyromagnetic ratio, n is the number density of atoms, V is the active volume, T_2 is the spin coherence time, and τ is the measurement time. A decade ago, for the traditional AM $T_2 \propto n^{-1}$ is dominated by the spin-exchange decoherence. For Rb atoms, we find the atom shot noise limited B-field sensitivity to be on the order of 1 fT/√Hz per cm$^{-3/2}$.

Comparing to an ideal inductive sensor: $\delta B = \sqrt{\frac{8\mu_0 kT\Delta\omega}{\omega^2 V\tau}}$

Here $\Delta\omega$ is the detection bandwidth and ω is the detection frequency. We find 1 fT/√Hz per cm$^{-3/2}$ sensitivity with 1-Hz bandwidth at room temperature only when the magnetic field noise is at frequency above 80 kHz.

Sandia National Laboratories

Spin-Exchange Decoherence

For I = 3/2 alkali-metal atoms in a magnetic field with negligible 2nd order Zeeman shifts, the relative populations of the hyperfine sublevels are:

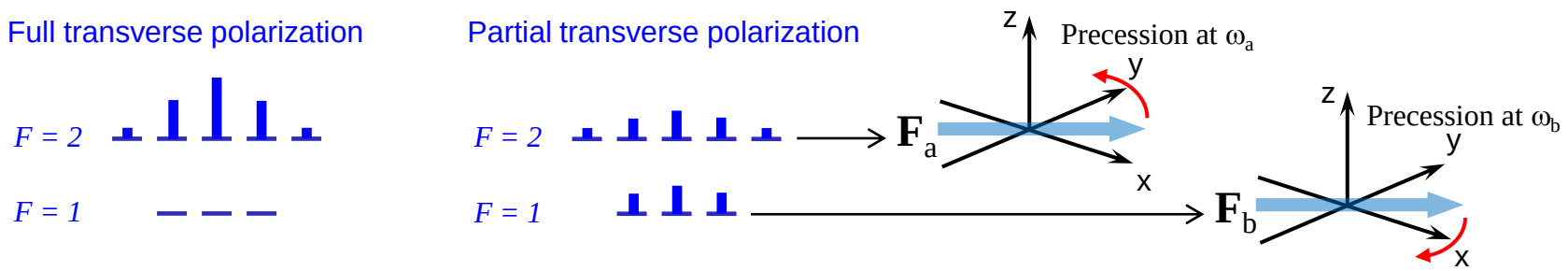

The hyperfine spin observable $\langle \mathbf{F} \rangle = \langle \mathbf{I} + \mathbf{S} \rangle$ has different precession rates from the upper and the lower manifold, where $\omega_b \sim -\omega_a$.

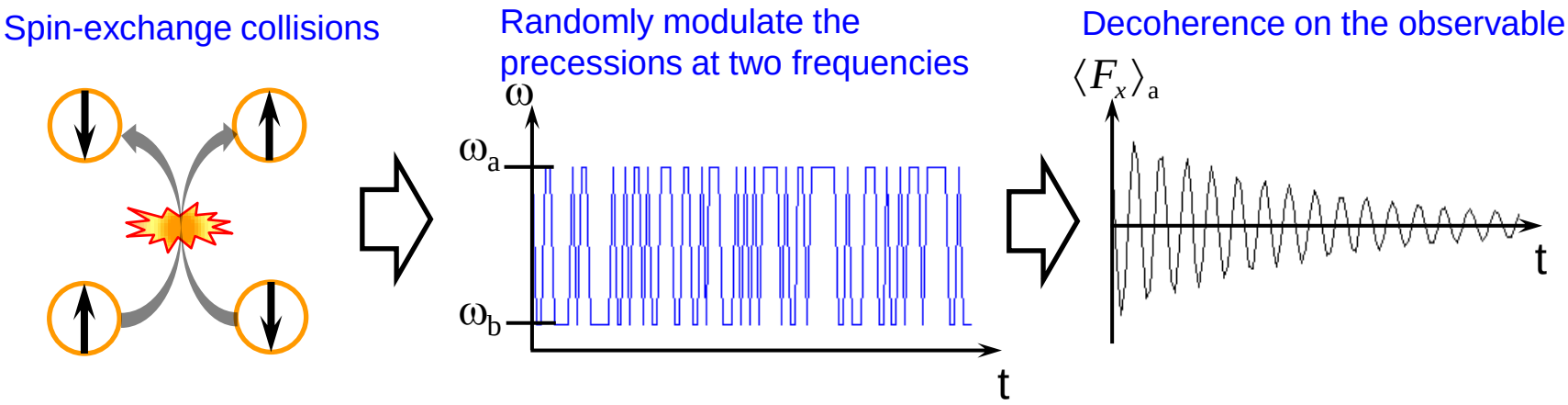

Sandia National Laboratories

Eliminating Spin-Exchange Decoherence

In 1973, Happer and Tang pointed out that the spin-exchange decoherence is strongly suppressed when the spin-exchange rate is much greater than the Larmor frequency. In 2002, Romalis *et. al.* took this advantage to make the first spin-exchange relaxation free (SERF) AM. The atom shot noise limit of the AM sensitivity is no longer limited by spin exchange but spin destruction due to collisions between alkali-metal atoms. The fundamental sensitivity can therefore be pushed down by 2–3 orders of magnitude.

Simple theoretical model:

With only spin-exchange mechanisms, the hyperfine spin evolutions of the two manifolds can be written as:

$$\frac{d}{dt}\langle F_+\rangle_a = i\omega_a\langle F_+\rangle_a + \Gamma_{\rm ex}(-\alpha_b\langle F_+\rangle_a + \alpha_a\langle F_+\rangle_b),$$
$$\frac{d}{dt}\langle F_+\rangle_b = i\omega_b\langle F_+\rangle_b + \Gamma_{\rm ex}(-\alpha_a\langle F_+\rangle_b + \alpha_b\langle F_+\rangle_a),$$

where the complex transverse spin $\langle F_+\rangle = \langle F_x\rangle + i\langle F_y\rangle$, and $\Gamma_{\rm ex}$ is the spin-exchange rate. The two coefficients α_a and α_b can be determined by detailed calculation, which gives $\alpha_a = \frac{2}{[I]^2}\frac{|\langle\mathbf{F}\rangle_a|}{|\langle\mathbf{S}\rangle|}$ and $\alpha_b = \frac{2}{[I]^2}\frac{|\langle\mathbf{F}\rangle_b|}{|\langle\mathbf{S}\rangle|}$, where $\mathbf{S}$ is the electron spin vector.

Sandia National Laboratories

Eliminating Spin-Exchange Decoherence

The solution of the previous equation can be represented by decaying an eigenvector, which has a form of $(A\langle F_+\rangle_a, B\langle F_+\rangle_b)\exp(-\Gamma t)$. By choosing ω_a=ω_0 and ω_b=-ω_0, we find complex decay rates as

$$\Gamma_\pm = \frac{\Gamma_{ex}}{2}\left((\alpha_a+\alpha_b) \mp \sqrt{(\alpha_a+\alpha_b)^2 - 4\frac{\omega_0^2}{\Gamma_{ex}^2} - 4\frac{\omega_0}{\Gamma_{ex}}(\alpha_a-\alpha_b)i}\right)$$

Using spin-temperature approximation, we find

$$\alpha_a = 2\frac{(I+1)\cosh(\beta(I+1))\sinh(\beta/2)) - \frac{1}{2}\sinh(\beta(I+1))\cosh(\beta/2))}{[I]^2\sinh(\beta[I]/2)\sinh^2(\beta/2)},$$

$$\alpha_b = 2\frac{I\cosh(\beta I)\sinh(\beta/2)) - \frac{1}{2}\sinh(\beta I)\cosh(\beta/2))}{[I]^2\sinh(\beta[I]/2)\sinh^2(\beta/2)},$$

where $[I] = 2I+1$, $\beta = \ln\left(\frac{1+P}{1-P}\right)$ is the spin-temperature parameter, and $P = 2|\langle \mathbf{S}\rangle|$ is the spin polarization.

One can quickly see that when Γ_{ex} >> ω_0, the slow-mode decay rate Γ_+ has highly suppressed spin-exchange effect!

Sandia National Laboratories

Spin-Exchange Effect on *I* = 3/2 atom as the ratio of Γ_{ex} and ω_0

The mechanism of spin-exchange decoherence suppression at $\Gamma_{ex} >> \omega_0$ is similar to motional narrowing phenomenon. The effective precession frequency ω is also shifted from ω_0. With 100% spin polarization, spin exchange plays no role at all.

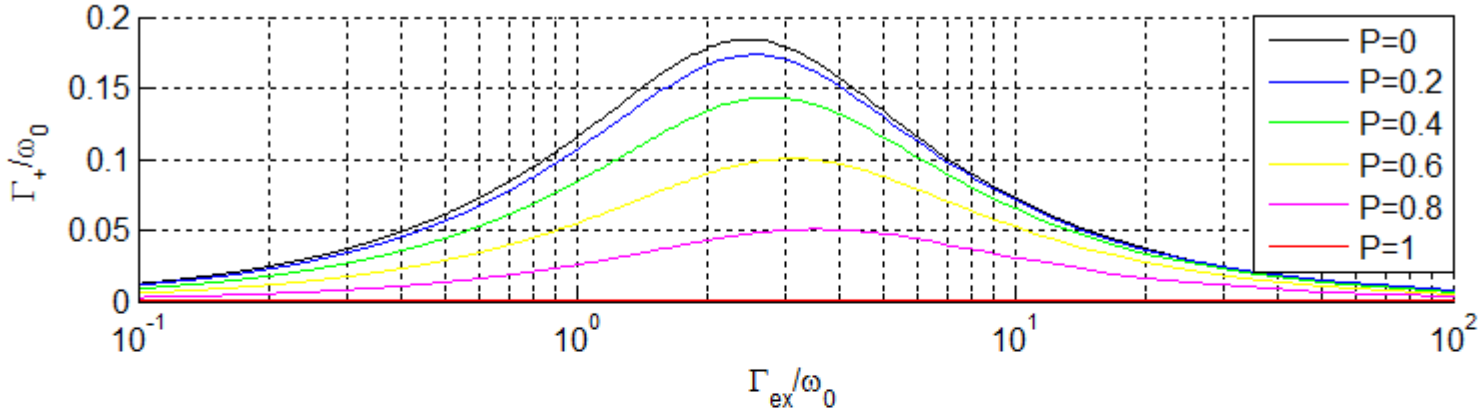

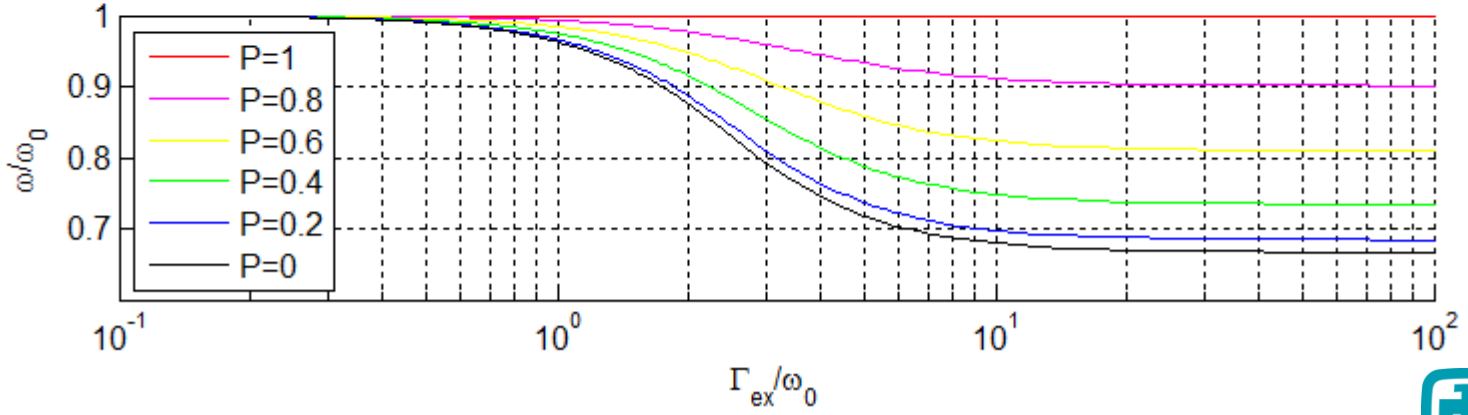

Sandia National Laboratories

Detailed Modeling for Atomic Vapor Cell

Atomic system of an alkali-metal vapor cell is a very dissipative system. A good approach is to use density-matrix calculations.

Schröedinger equation for the i-th atom in an atomic ensemble is given by

$$i\hbar\frac{d}{dt}|\psi_i\rangle = H_i|\psi_i\rangle,$$

where $|\psi_i\rangle = |\psi_i(t)\rangle$ represents the atomic quantum state of an alkali-metal atom, and $H_i = H^{(0)} + H^{(1)} + H_i^{(2)}$ is the total Hamiltonian for each atom. Here $H^{(0)}$ is a time-independent "unperturbed" Hamiltonian, and $H^{(1)} = H^{(1)}(t)$ is a time-dependent purturbation representing the interaction of the atom with the optical pumping, microwave, and RF fields. Both $H^{(0)}$ and $H^{(1)}$ are identical for all atoms. The collisional interaction of the ith atom is represented by the time-dependent Hamiltonian $H_i^{(2)} = H_i^{(2)}(t)$. The density matrix of an ensemble of N identical atoms can be described by

$$\rho = \frac{1}{N}\sum_i |\psi_i\rangle\langle\psi_i|.$$

Sandia National Laboratories

Density Matrix in Interaction Picture

The density matrix in the interaction frame, $\tilde{\rho}$ is defined by $\rho = \mathrm{e}^{\frac{1}{i\hbar}H^{(0)}t}\tilde{\rho}\,\mathrm{e}^{-\frac{1}{i\hbar}H^{(0)}t}$.

The evolution operator of a collisional event for $\tilde{\rho}$: $\widetilde{U}_i = \exp\left(\frac{1}{i\hbar}\int_t^{t+\delta t}\widetilde{H}_i^{(2)}(t')dt'\right)$.

The collision time scale is δt and $H_i^{(2)}\delta t/\hbar \ll 1$.

Because collisions are uncorrelated and the interaction time scale δt is very short, we find the time derivative of $\tilde{\rho}$ to be

$$\left[\frac{d\tilde{\rho}}{dt}\right]^{(2)} = \mathcal{N}\left\langle \widetilde{U}_i\tilde{\rho}\,\widetilde{U}_i^{\dagger} - \tilde{\rho}\right\rangle,$$

where $\mathcal{N}$ is the number of collisions occurred per unit time in an ensemble system, and $\langle\ \rangle$ denotes the ensemble average over all possible types of collisions, for example, over all impact parameters and orbital directions. We can expand $\widetilde{U}_i$ into

$$\begin{aligned}\widetilde{U}_i &= 1 + \frac{1}{i\hbar}\int_{-\infty}^{\infty}\widetilde{H}_i^{(2)}(t')\,dt' + \frac{1}{2}\left(\frac{1}{i\hbar}\int_{-\infty}^{\infty}\widetilde{H}^{(2)}(t')_i\,dt'\right)^2 + \cdots \\ &= 1 - i\Theta_i - \frac{1}{2}\Theta_i^2 + \cdots.\end{aligned}$$

Because $\langle\Theta_i\rangle \ll 1$, to the second order of $\tilde{U}_i$, we have

$$\left[\frac{d\tilde{\rho}}{dt}\right]^{(2)} = \mathcal{N}\left[-i[\,\langle\Theta_i\rangle,\tilde{\rho}\,] + \langle\Theta_i\tilde{\rho}\Theta_i\rangle - \frac{1}{2}\{\,\langle\Theta_i\Theta_i\rangle,\tilde{\rho}\,\}\right]$$

Lindblad form

Sandia National Laboratories

Important Collisional Interactions in Atomic Magnetometer System

A simple form of density-matrix equation with one kind of collisional interaction:

$$\frac{d\rho}{dt} = \frac{1}{i\hbar}[H^{(0)}, \rho] + \frac{1}{i\hbar}[H^{(1)}, \rho] + \mathcal{N}\left[-i[\langle\Theta\rangle, \rho] + \langle\Theta\rho\Theta\rangle - \frac{1}{2}\{\langle\Theta\Theta\rangle, \rho\}\right]$$

Ground-state spin destruction (S-damping):

$$H_{\mathrm{sd}}^{(2)} = \gamma(r)\mathbf{N}\cdot\mathbf{S} \qquad \dot{\rho}_{\mathrm{sd}} = \Gamma_{\mathrm{sd}}(\varphi - \rho), \quad \varphi = \rho/4 + \mathbf{S}\cdot\rho\mathbf{S}$$

Ground-state spin exchange:

$$H_{\mathrm{ex}}^{(2)} = J(r)\mathbf{S}'\cdot\mathbf{S} \qquad \dot{\rho}_{\mathrm{ex}} = \frac{1}{i\hbar}[\delta\mathcal{E}_{\mathrm{ex}}, \rho] + \Gamma_{\mathrm{ex}}[\varphi(1 + 4\langle\mathbf{S}\rangle\cdot\mathbf{S}) - \rho]$$

Excited-state J-damping:

$$H_{\mathrm{jd}}^{(2)} = \gamma_j(r)\mathbf{N}\cdot\mathbf{J} \qquad \dot{\rho}_{\mathrm{jd}}^{(e)} = \Gamma_{\mathrm{jd}}\left(\mathbf{J}\cdot\rho^{(e)}\mathbf{J} - \frac{1}{2}\{\mathbf{J}\cdot\mathbf{J}, \rho^{(e)}\}\right)$$

Excited state quenching to ground state:

$$\frac{d}{dt}\rho^{(g)} = \Gamma_{\mathrm{q}}\left(\frac{1}{4}U\rho^{(e)}U^{\dagger} + \mathbf{A}\cdot\rho^{(e)}\mathbf{A}^{\dagger}\right)$$

Atom diffusion inside the vapor cell with buffer gases:

$$\frac{\partial\rho(\mathbf{r})}{\partial t} = D\nabla^2\rho(\mathbf{r})$$

Sandia National Laboratories

Density Matrix Modeling for Spin-Exchange Effect

Low transverse spin polarization, weak optical pumping

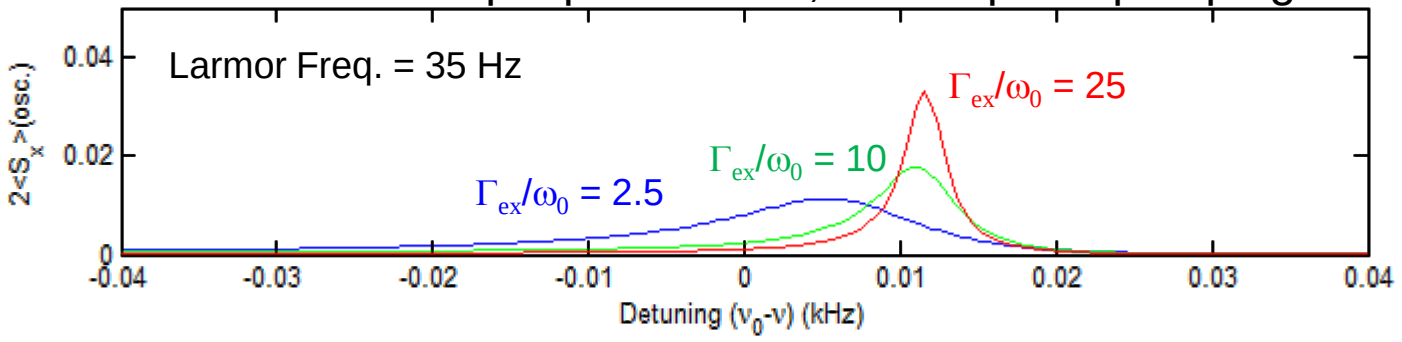

High transverse spin polarization, strong optical pumping

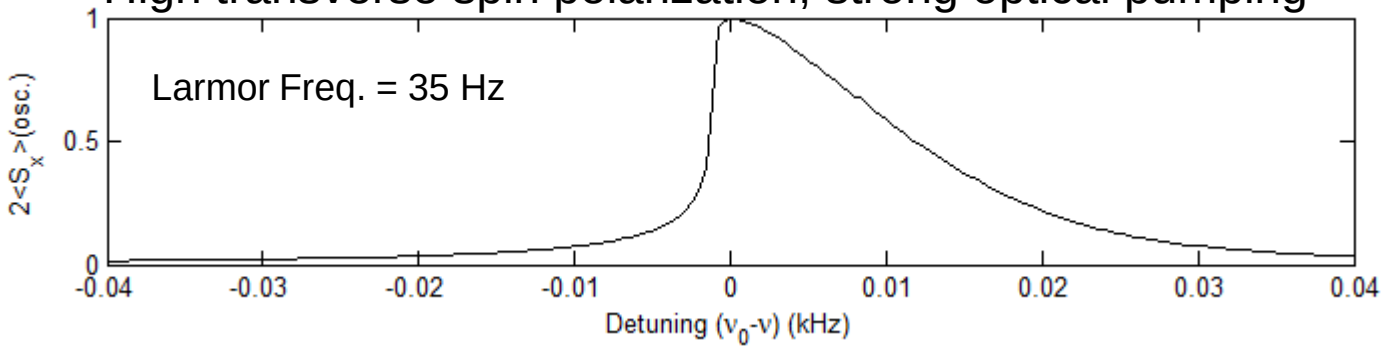

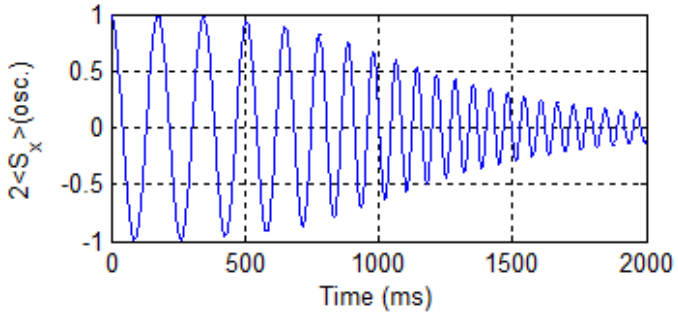

Exp. Data from PRL 106 143601 (2011)

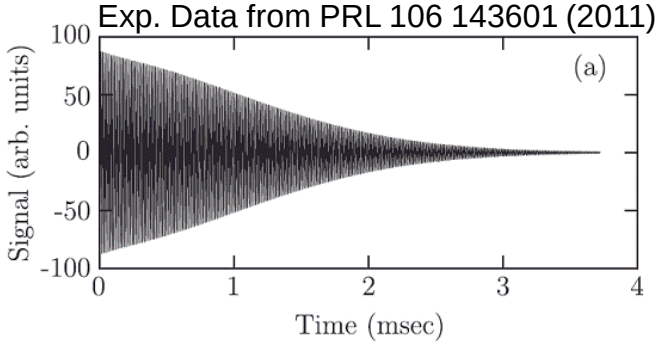

Sandia National Laboratories

Spin Relaxation and Buffer Gases

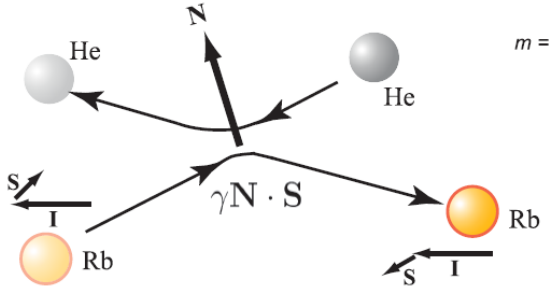

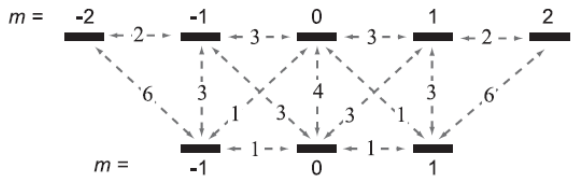

	He	Ne	Ar	Kr	Xe	N_2
Li	—	—	—	—	—	—
Na	0.0036 327°C [71]	(0.18)	(200)	(72)	1090 180°C [72]	—
K	0.005 150°C [73]	(0.16)	6.3 117°C [74]	(190)	(1800)	0.75 150°C [75]
Rb	0.087 150°C [76]	(0.18)	6.1 27°C [57]	270 27°C [57]	2200 150°C [77]	1.0 70°C [78]
Cs	0.24 0°C [81]	(0.20)	10.4 0°C [79]	260 ?°C [80]	(2300)	5.5 15°C [81]

Electron-spin randomization cross sections, 10^{-22} cm^2

	^{4}He	Ne	Ar	Kr	Xe	N_2
Li	—	—	—	—	—	—
Na	0.92 155°C [96]	0.5 155°C [96]	0.28 155°C [96]	—	—	0.54 155°C [96]
K	0.45 52°C [97]	0.19 27°C [97]	0.31 117°C [74]	—	—	—
Rb	0.35 80°C [77]	0.16 27°C [98]	0.14 27°C [98]	0.12 27°C [57]	0.13 47°C [99]	0.159 60°C [100]
Cs	0.39 27°C [101]	0.15 0°C [102]	0.13 0°C [102]	0.14 27°C [103]	—	0.12 27°C [104]

Diffusion coefficients (in cm^2 s^{-1})

Sandia National Laboratories

Radiation Trapping

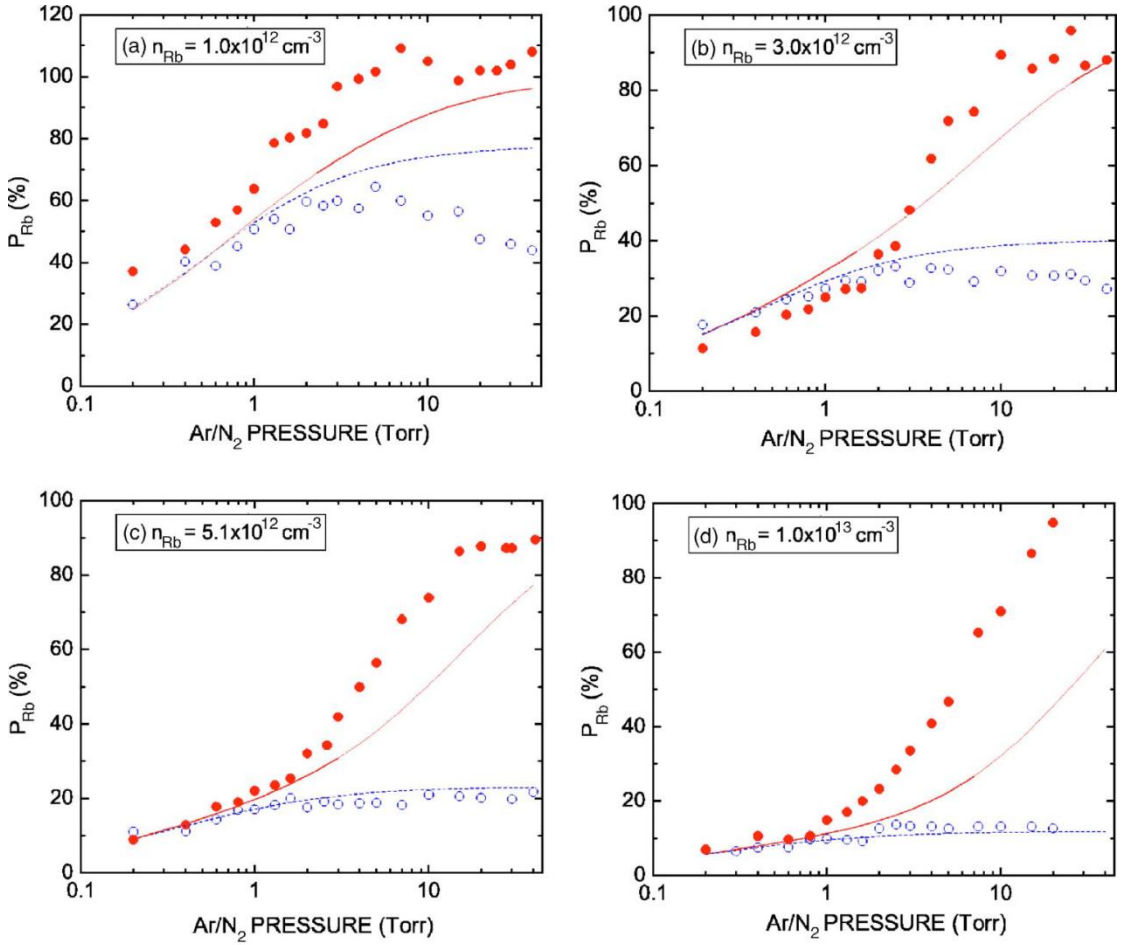

- Radiation trapping is due to the spontaneous emitted photons being absorbed by other atoms in the ensemble
- Noble gases cannot efficiently quench the excited atoms without photon emissions
- Nitrogen is a good quenching molecule
- To suppress radiation trapping, we need to add enough quenching gas, which gives quenching rate surpassing the spontaneous decay rate. For N_2, it is usually above a few torr.

Experimental data from PRA 75 023401 (2007).
Solid circle: N_2 and open circle: Ar.

Sandia National Laboratories

Probing the Spin Resonance at Nearly Zero B_z Field

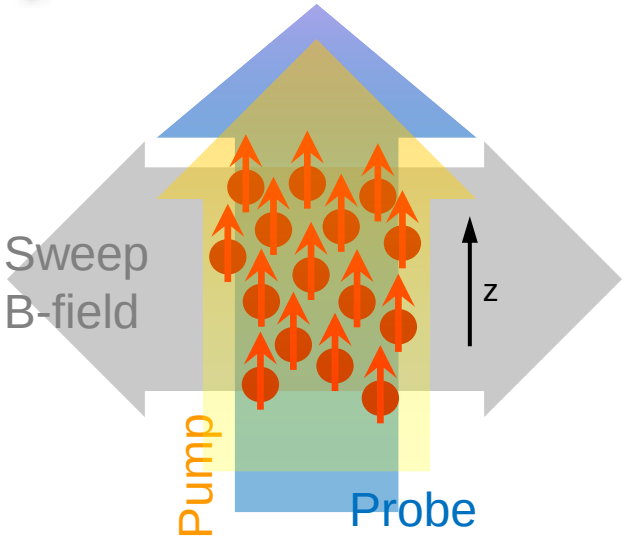

Rotation of the probe polarization

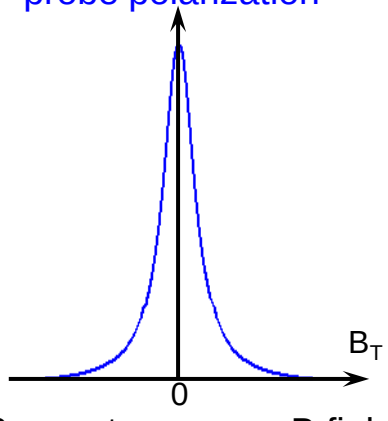

Sweep transverse B field

Adding a small modulation to the transverse direction, we obtain the transverse magnetic field amplitude from the demodulation of the probe signal.

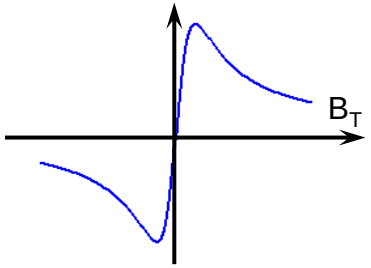

A simple mathematical description of this system:

$$\langle \dot{\mathbf{F}} \rangle = -\frac{1}{T_2}(\langle F_x \rangle \mathbf{x} + \langle F_y \rangle \mathbf{y}) + \frac{1}{T_1}(F_{\max} - \langle F_z \rangle)\mathbf{z} + \gamma \mathbf{B} \times \langle \mathbf{F} \rangle$$

Here, $F_{\max} = \frac{R_{\rm op}}{R_{\rm op}+R_{\rm sr}} F$ is the maximum spin magnitude can be achieved by optical pumping with spin-exchange free condition. $R_{\rm op}$ and $R_{\rm sr}$ are the effective pumping rate and the total spin relaxation rate of the hyperfine spin system.

In most previous AM studies, people assume $T_2 = T_1 = T$, with this condition, we can find the steady-state solutions:

$$\langle F_x \rangle = \frac{\gamma B_y T F_{\max}}{1+\gamma^2(B_x^2+B_y^2)T^2}$$

$$\langle F_y \rangle = -\frac{\gamma B_x T F_{\max}}{1+\gamma^2(B_x^2+B_y^2)T^2}$$

$$\langle F_z \rangle = \frac{F_{\max}}{1+\gamma^2(B_x^2+B_y^2)T^2}$$

Sandia National Laboratories

Buffer Gas, Pressure, and Temperature for Rb Vapor Cell

Neon buffer gas

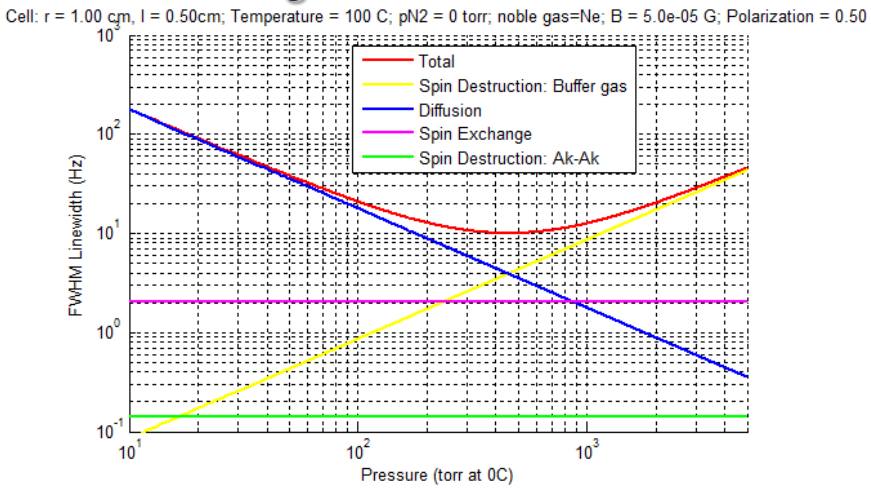

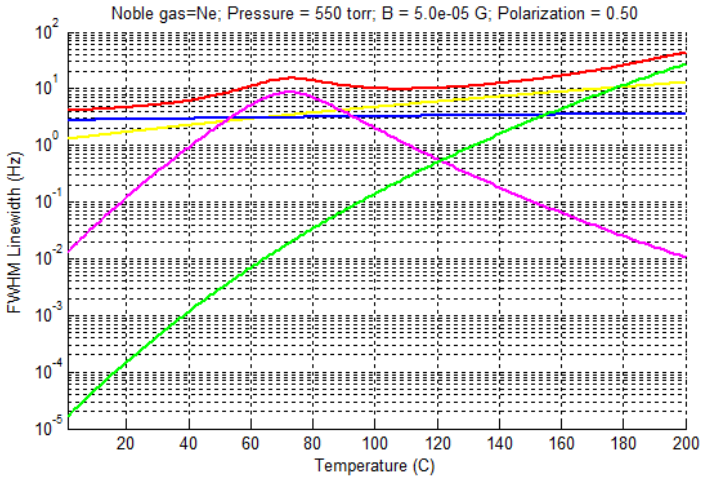

Nitrogen buffer gas

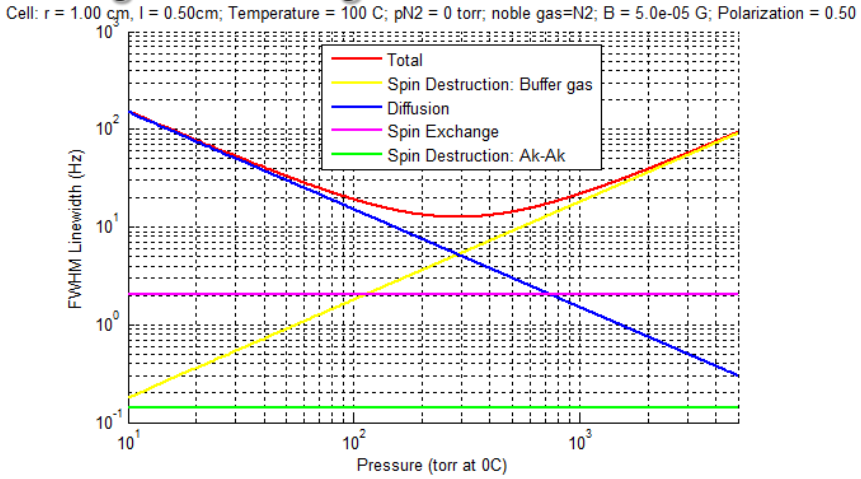

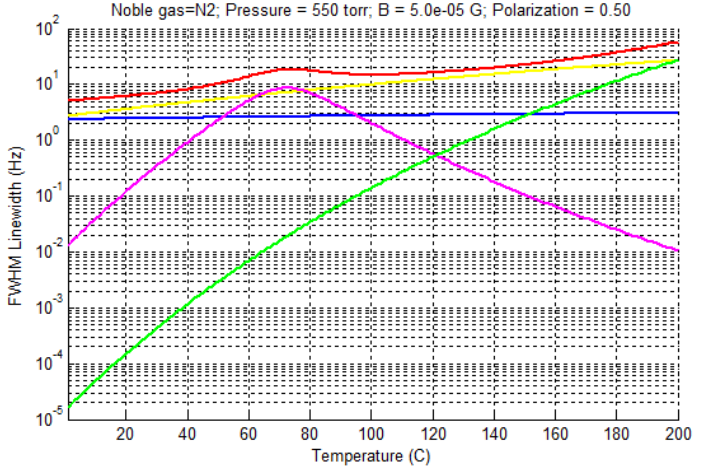

Sandia National Laboratories

AM Results Using 5-mm Thick ^{87}Rb Cell with Ne Buffer Gas

The best sensitivity we got was only 72 fT/√Hz.

The result was too bad! so we did not save any data.

Sandia National Laboratories

Excited Alkali-Metal Atoms Colliding with Buffer Gas

An excited Rb atom collides with a molecule:

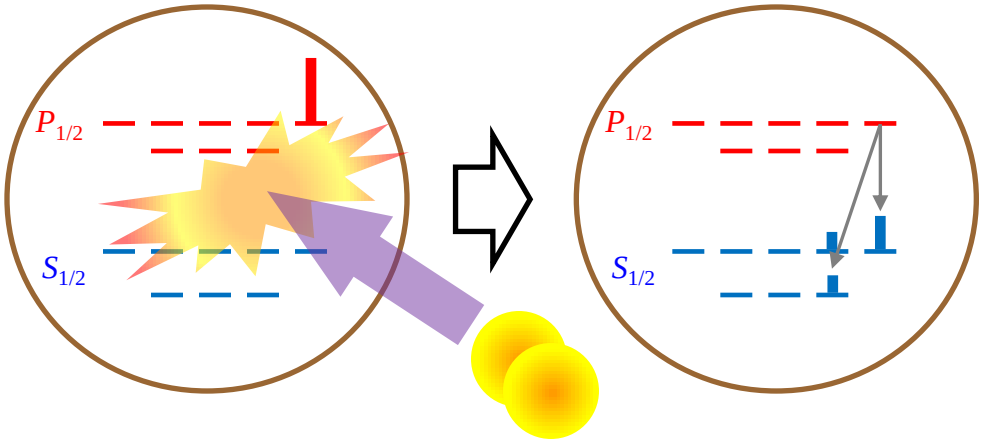

- A quenching collision makes the atom decay back to ground state without emitting a photon.
- Quenching randomizes the electron spin but preserve the nuclear spin.

- Non-quenching collisions make spin relaxation (J-damping) in the excited state .
- This reduces optical pumping efficiency.

An excited Rb atom collides with an atom:

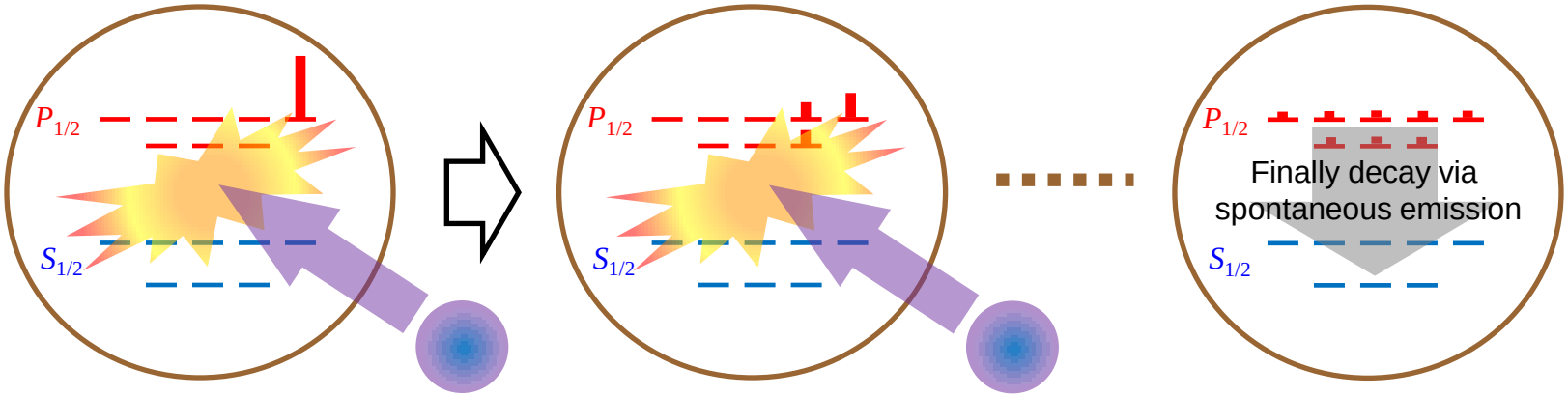

Sandia National Laboratories

Photon Cost for Fully Spin Polarizing ^{87}Rb with N_2 and Ne Buffer Gases

Photon cost map using broadband optical pumping

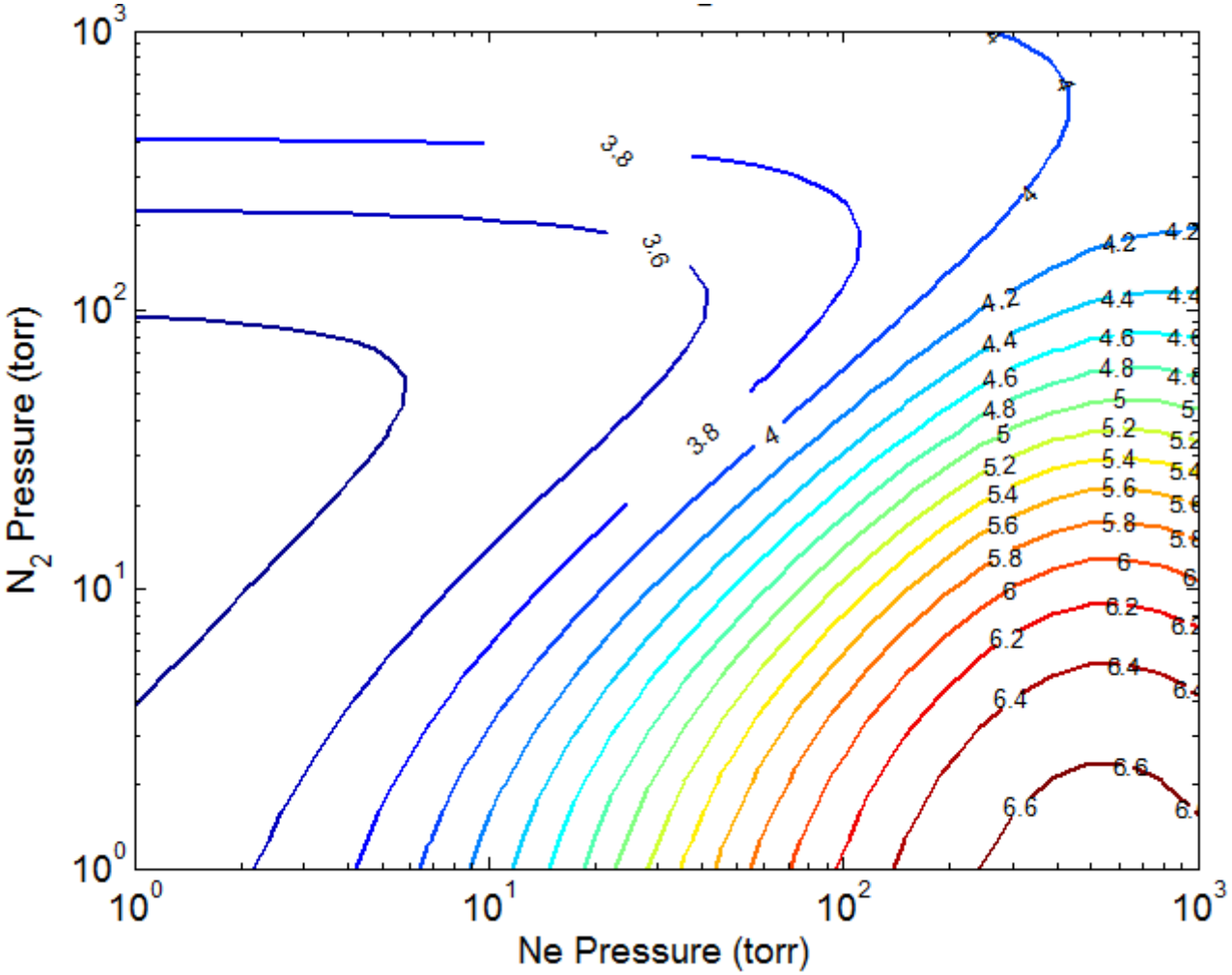

Sandia National Laboratories

Detuning Scan of the Pump Laser Using Rb Cell with Ne Buffer Gas

Looking for the optimal pump laser detuning, which has maximum signal-size/linewidth. At different detunings, we adjust the laser power to maintain the signal size.

Experimental Data

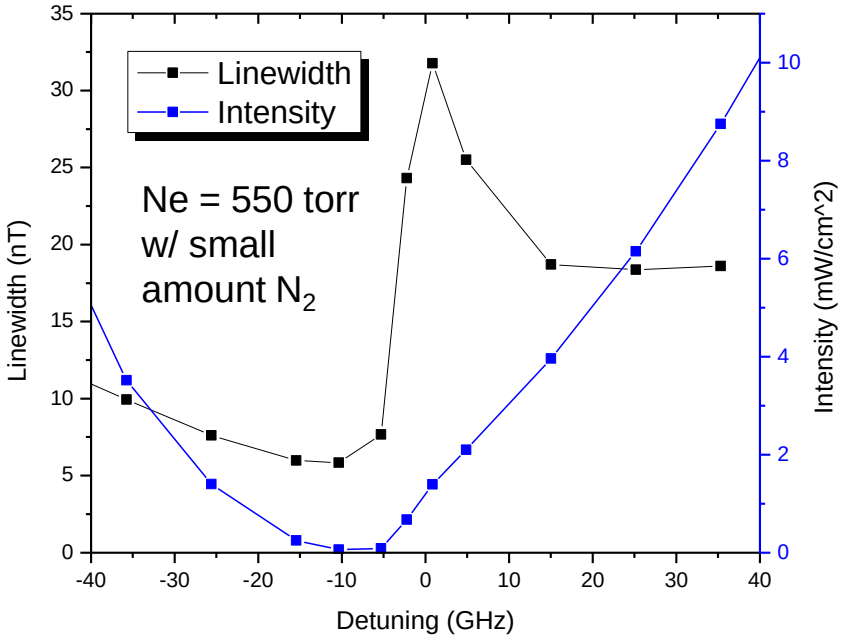

Density-Matrix Modeling

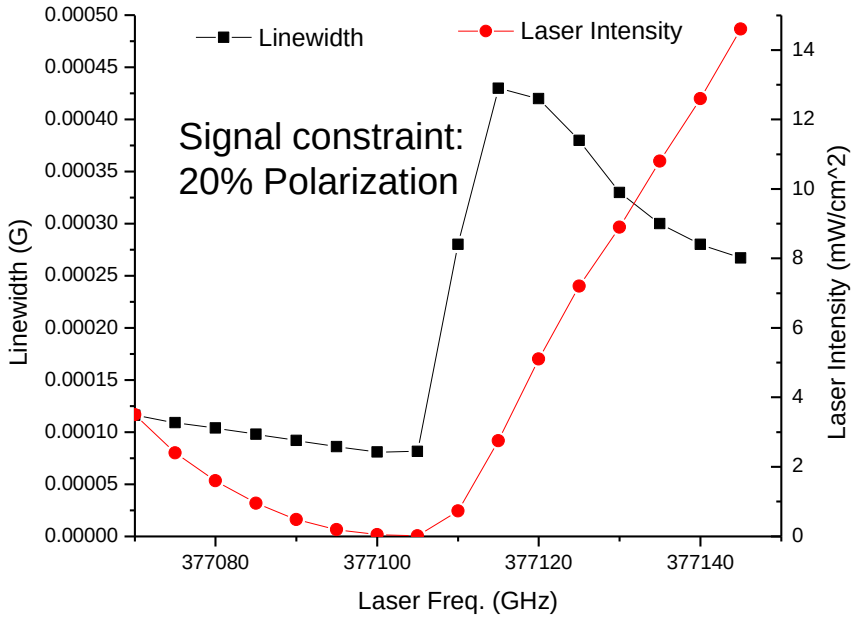

Sandia National Laboratories

Detuning Scan of the Pump Laser Using Rb Cell with N_2 Buffer Gas

Nitrogen buffer gas leads to a much stronger signal with narrower linewidth and much lower laser power consumption.

Experimental Data

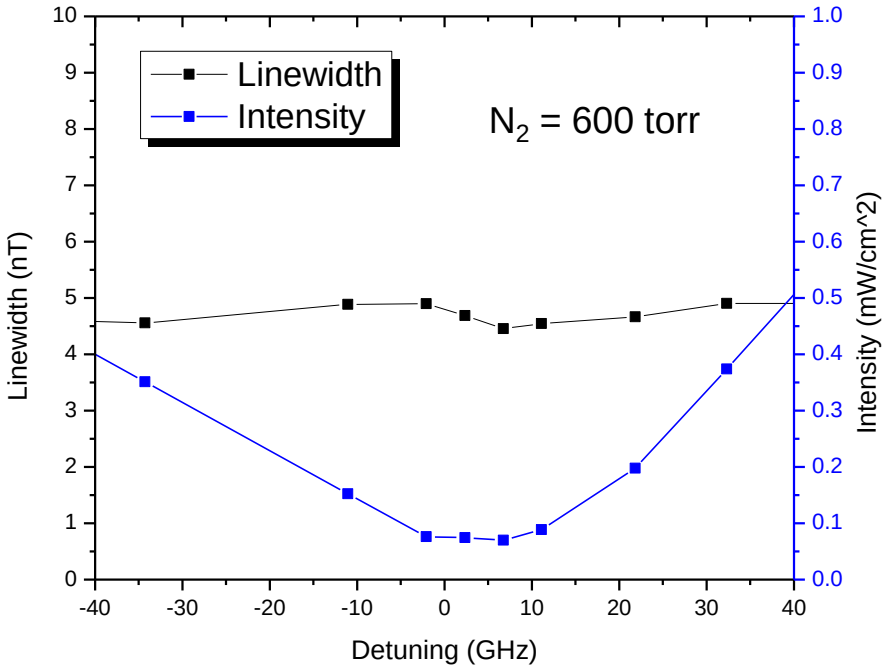

Density-Matrix Modeling

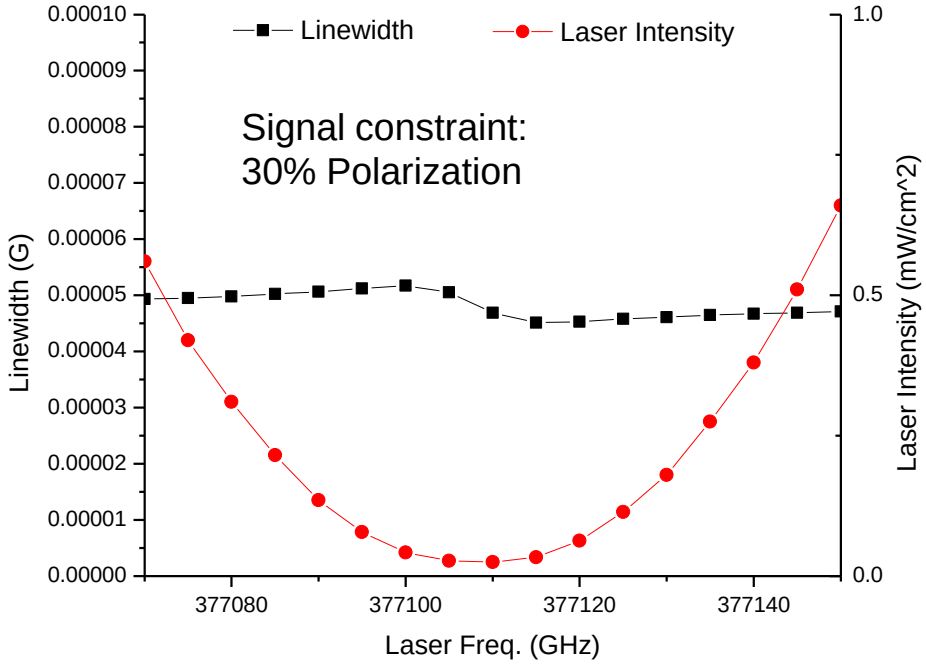

Sandia National Laboratories

Atomic Magnetometer Experimental Setup

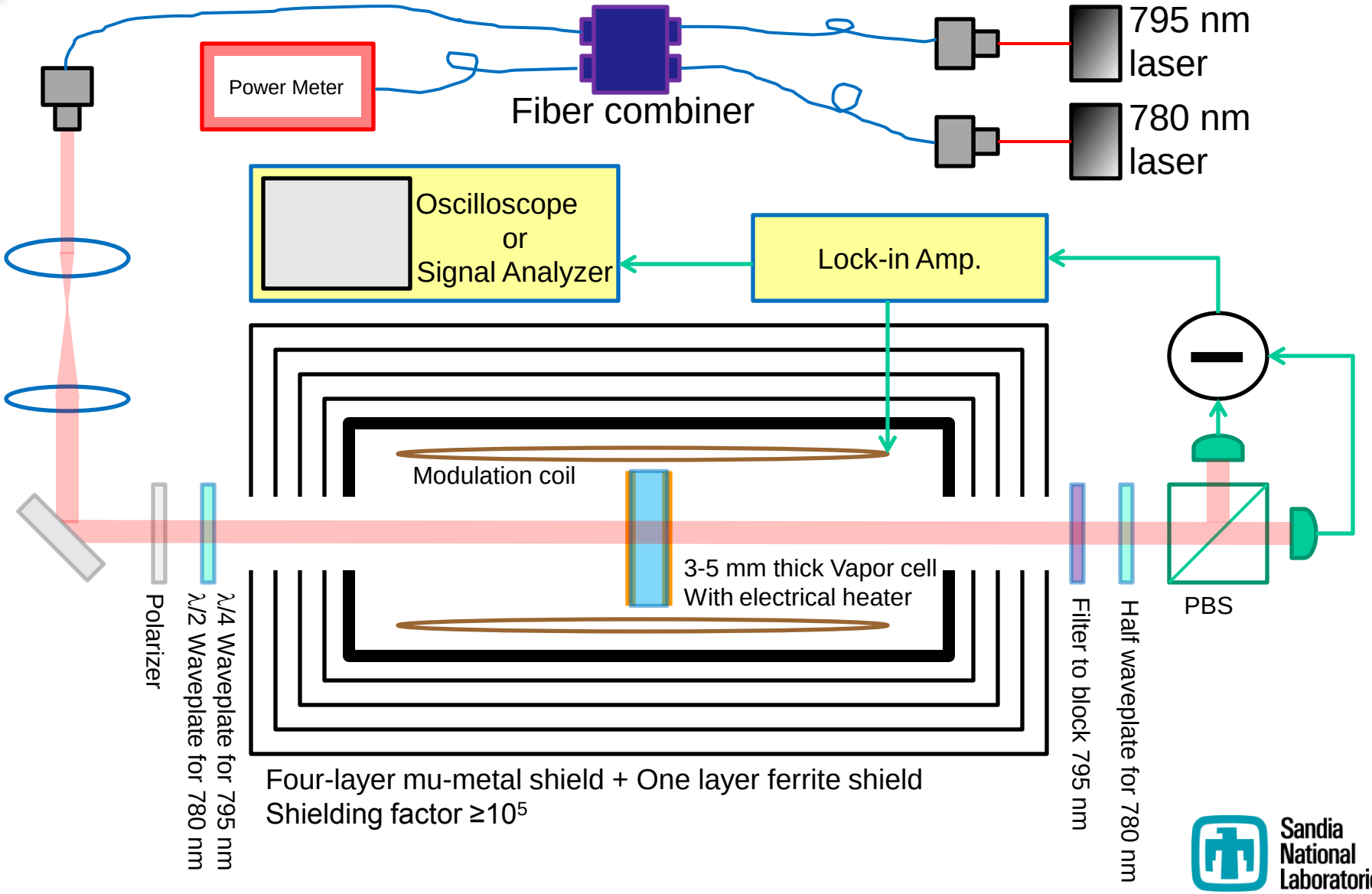

Sandia National Laboratories

Theoretical Modeling with Spatial Effect

Alkali-metal atom: 87; buffer gas: N2 torr; Temperature = 160 C; Cell r = 1 cm, l = 0.5 cm; B-field = 5e-05 G

Incoming pumping peak intensity = 35 mW/cm^2; vapor-cell optical depth = 0.025 cm; absorption cross section = 2.3341e-13 cm^2; pump beam width (FWHM) = 0.25 cm; probe beam width (FWHM) = 0.25 cm

Total pumping intensity distribution

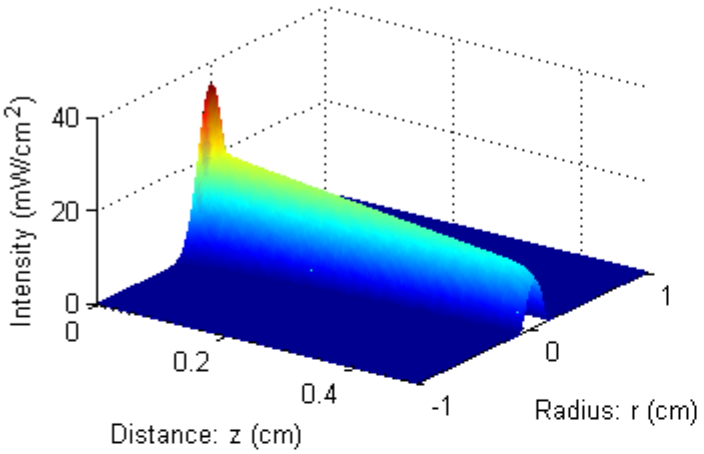

Polarization distribution as a contour plot

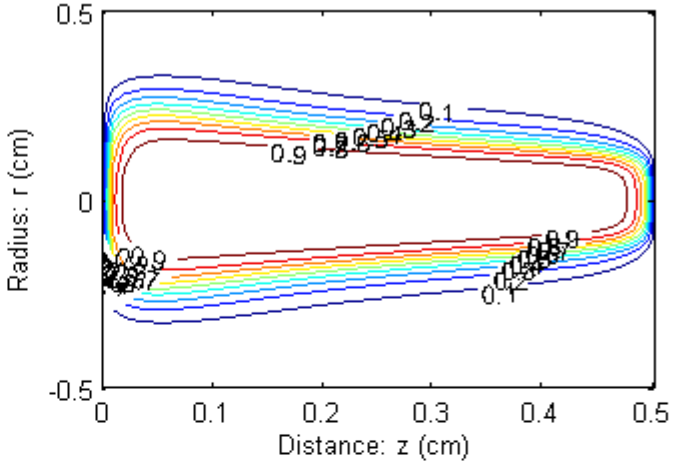

Linewidth (FWHM) distribution as a contour plot

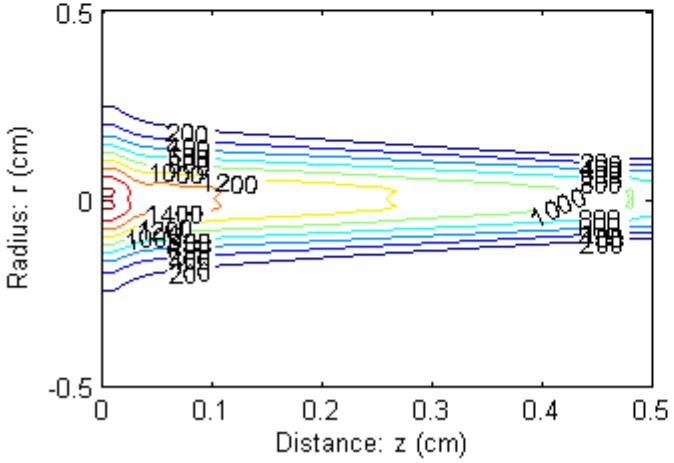

Gyromagnetic ratio (kHz/G) distribution as a contour plot

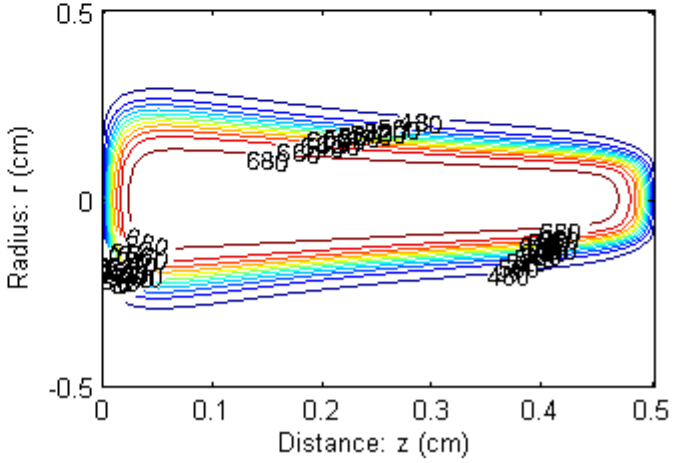

Sandia National Laboratories

Looking for Optimal Operating Parameters from Theoretical Modeling

Alkali-metal atom: 87; Temperature = 160 C; Cell r = 1 cm, l = 0.5 cm; B-field = 5e-05 G; vapor-cell optical depth = 0.025 cm; pump beam width (FWHM) = 0.24977 cm; probe beam width (FWHM) = 0.24977 cm

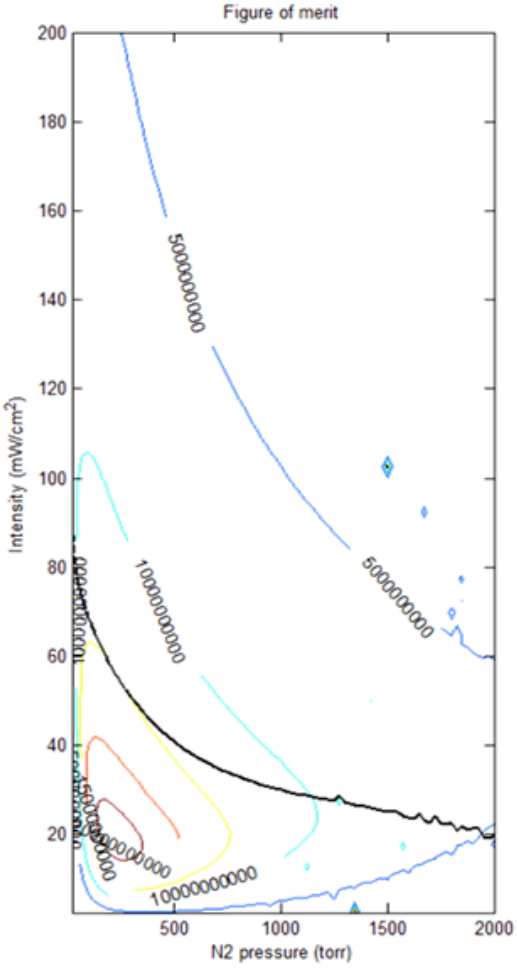

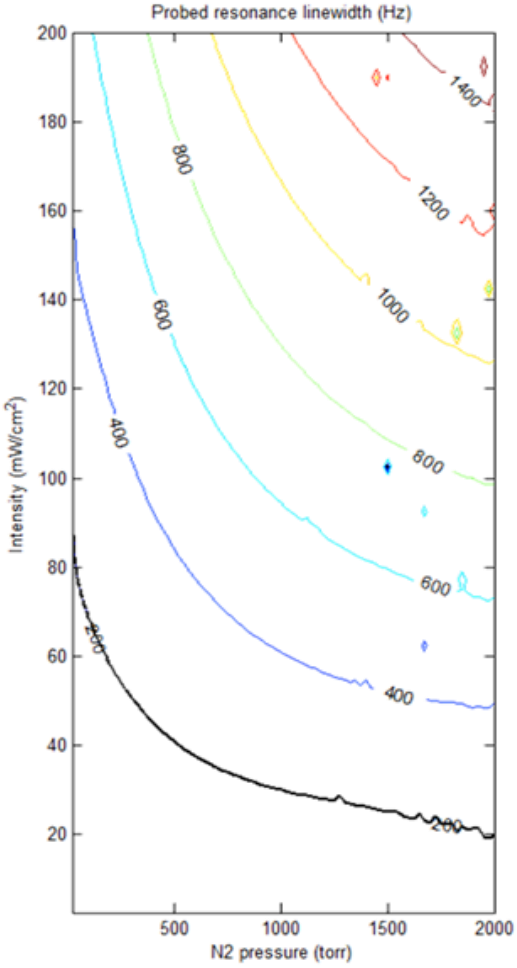

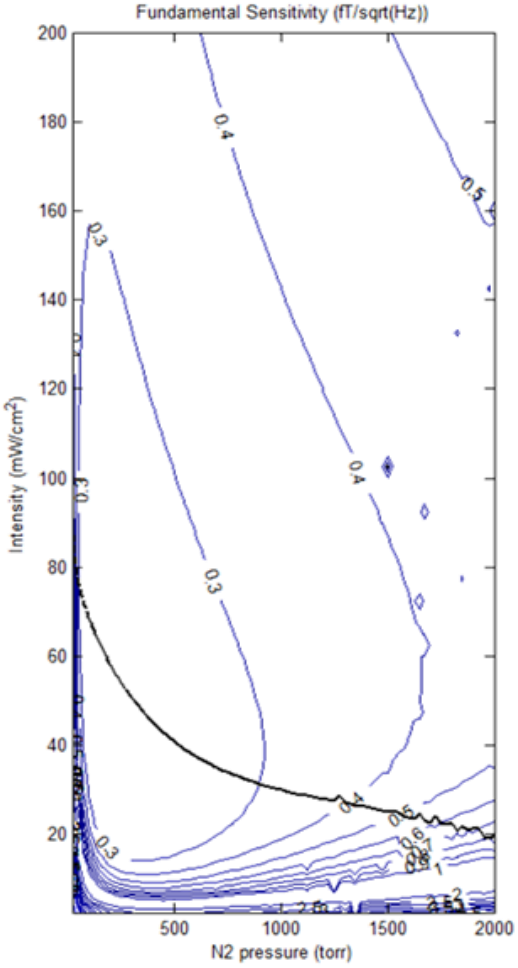

Sandia National Laboratories

Performance of Sandia Atomic Magnetometer with 0.025 cm^3 active volume

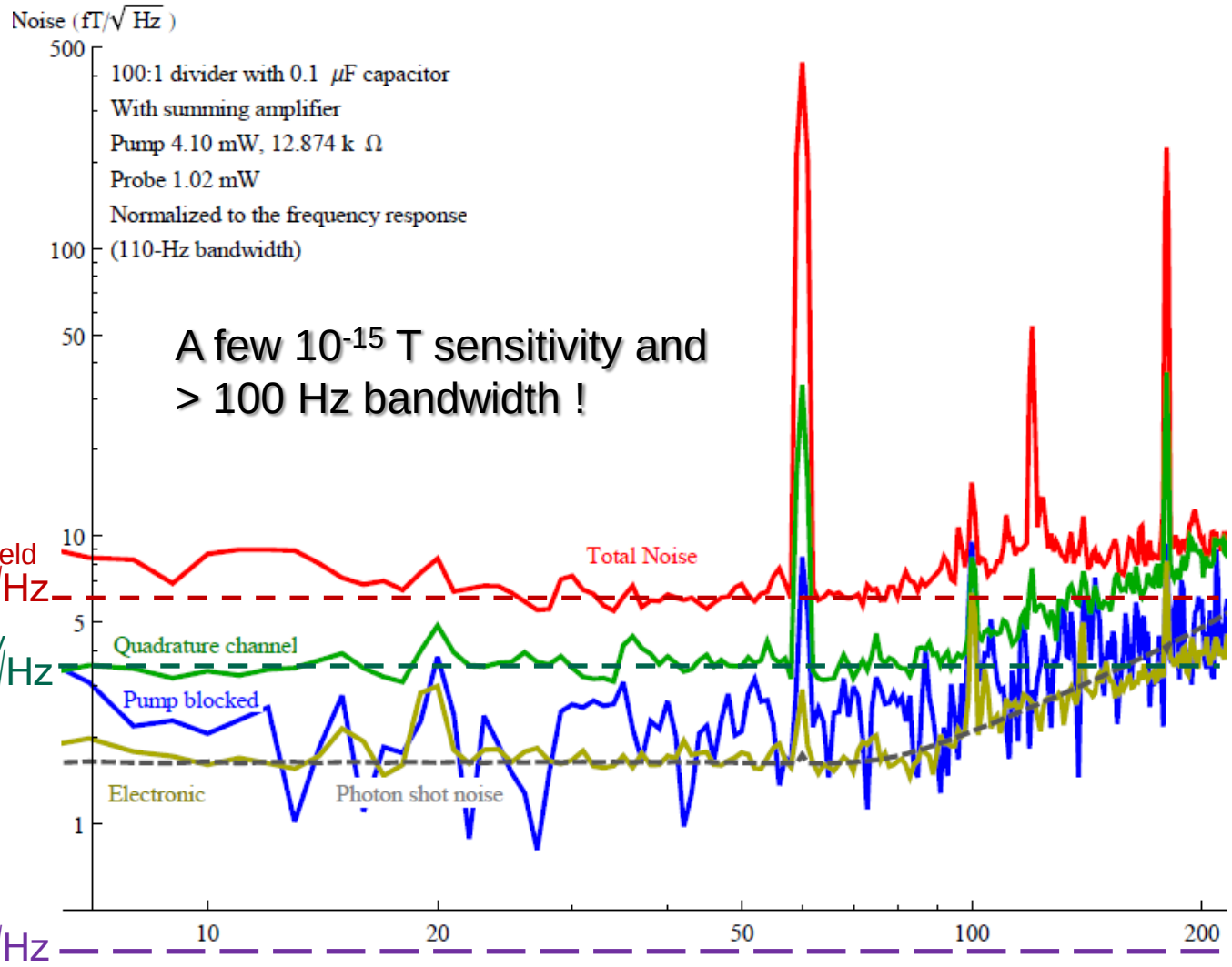

B-field noise inside the shield
6 fT/√Hz

Technical B-field sensitivity
3.3 fT/√Hz

Atom shot noise limit
0.3 fT/√Hz

Sandia National Laboratories

Summary

- Comparing to SQUID magnetic-field sensors, atomic magnetometers (AMs) do not need cryogenic system to maintain liquid helium temperature. Therefore, AM systems can have lower complexity, more portable, shorter sensing distance from the sample, and much lower operating cost.
- Highly sensitive atomic magnetometry with broad detection bandwidth and small active volume has great advantage for biomagnetic detections.
- Detailed modeling shows that the strong spin relaxation due to the collisions between excited alkali-metal atoms and noble-gas atoms significantly degrade the performance of atomic magnetometry. A good quenching gas, such as N_2, not only reduces radiation trapping but also helps optical pumping efficiency. This increases the SNR, relax the power budget for an AM array system, and allows us to operate the vapor cell at higher temperature.
- Nitrogen is the best buffer gas for miniature AMs.
- We have demonstrated several $fT/Hz^{1/2}$ sensitivity and greater than 100-Hz measurement bandwidth from a 0.025 cm^3 active volume.

Acknowledgement

- Dr. Peter Schwindt (PI of the current AM MEG project at Sandia)
- Dr. Anthony Colombo (Postdoc of the current AM MEG project at Sandia)
- Mr. Tony Carter (Technician of the current AM MEG project at Sandia)
- Dr. Cort Johnson (Draper Laboratory, Staff of former AM project at Sandia)
- Dr. Mike Weisend (MEG expert, Wright State University)
- Dr. Jim McKay (MEG signal processing specialist, Candoo Systems)

Sandia National Laboratories